

Impact of the Ce $4f$ states in the electronic structure of the intermediate-valence superconductor CeIr₃

Shin-ichi Fujimori¹, Ikuto Kawasaki¹, Yukiharu Takeda¹,
Hiroshi Yamagami^{1,2}, Norimasa Sasabe³, Yoshiki J. Sato^{4,5},
Ai Nakamura⁴, Yusei Shimizu⁴, Arvind Maurya^{4,6},
Yoshiya Homma⁴, Dexin Li⁴, Fuminori Honda^{4,7}, and Dai Aoki⁴

¹ Materials Sciences Research Center, Japan Atomic Energy Agency, Sayo, Hyogo 679-5148, Japan

² Department of Physics, Faculty of Science, Kyoto Sangyo University, Kyoto 603-8555, Japan

³ Japan Synchrotron Radiation Research Institute, SPring-8, Sayo, Hyogo 679-5148, Japan

⁴ Institute for Materials Research, Tohoku University, Oarai, Ibaraki 311-1313, Japan

⁵ Department of Physics, Faculty of Science and Technology, Tokyo University of Science, Noda, Chiba 278-8510, Japan

⁶ Department of Physics, School of Physical Sciences, Mizoram University, Aizawl 796 004, India

⁷ Central Institute of Radioisotope Science and Safety Management, Kyushu University, Motooka 744, Fukuoka Nishi, Fukuoka 819-0395, Japan

E-mail: fujimori@spring8.or.jp

8 November 2023

Abstract. The electronic structure of the f -based superconductor CeIr₃ was studied by photoelectron spectroscopy. The energy distribution of the Ce $4f$ states were revealed by the Ce $3d - 4f$ resonant photoelectron spectroscopy. The Ce $4f$ states were mostly distributed in the vicinity of the Fermi energy, suggesting the itinerant character of the Ce $4f$ states. The contribution of the Ce $4f$ states to the density of states (DOS) at the Fermi energy was estimated to be nearly half of that of the Ir $5d$ states, implying that the Ce $4f$ states have a considerable contribution to the DOS at the Fermi energy. The Ce $3d$ core-level and Ce $3d$ X-ray absorption spectra were analyzed based on a single-impurity Anderson model. The number of the Ce $4f$ states in the ground state was estimated to be $0.8 - 0.9$, which is much larger than the values obtained in the previous studies (i.e., $0 - 0.4$).

1. Introduction

CeIr₃ is a *f*-based superconductor with a relatively high transition temperature ($T_{\text{SC}} = 3.1$ K), and its superconducting properties have attracted much attention in recent years [1, 2, 3, 4]. Its thermodynamical properties and μSR measurements suggest CeIr₃ is a weak-coupling superconductor with an anisotropic *s*-wave gap [1, 4]. One of the key issues of this compound is the role of the Ce 4*f* states in superconductivity. Isostructural analogue compounds LaIr₃ ($T_{\text{SC}} = 2.5$ K [5, 6]) and ThIr₃ ($T_{\text{SC}} = 4.41$ K [7]) also exhibit the superconductivity with similar or higher transition temperatures; hence, the role of the Ce 4*f* states in the superconductivity of CeIr₃ is considered to be negligible [8]. Experimentally, the Ce 4*f* states in CeIr₃ are suggested as an intermediate-valence state, but the occupancy of the 4*f* states n_{4f} is a matter of controversies. Based on the relationship between the transition temperature and the valence states in (La, Th)Ir₃ alloys, n_{4f} is estimated as $n_{4f} \sim 0.4$ [9]. Górnicka *et al* recently suggested that $n_{4f} \sim 0$ based on the weak-temperature-dependent magnetic susceptibility of CeIr₃. They argued that the contributions from the Ce 4*f* states at the Fermi energy are negligible in this compound [2]. On the contrary, the experimental specific heat coefficient ($\gamma_{\text{exp}} = 25.1$ mJ/mol · K²) is much larger than that obtained by the GGA calculation ($\gamma_{\text{GGA}} = 10.2$ mJ/mol · K²) [2], suggesting that there should be a considerable contribution from the correlated Ce 4*f* states at the Fermi energy. Gutowska *et al* recently calculated the electronic structure of CeIr₃ based on the dynamical mean field theory (DMFT) and reproduced the experimental specific heat coefficient and the electron–phonon coupling [10]. Their calculation showed that the Ce 4*f* states had a finite contribution at the Fermi energy, and its occupation number was $n_{4f} \sim 0.8$. Thus, the nature of the Ce 4*f* states of this compound is controversial.

In this study, we have investigated the Ce 4*f* states of CeIr₃ by the Ce 3*d* – 4*f* resonant photoelectron spectroscopy (RPES), X-ray absorption spectroscopy (XAS), and core-level photoelectron spectroscopy. Accordingly, the RPES study shows that the Ce 4*f* states form a sharp peak at the Fermi energy, suggesting that the Ce 4*f* states in CeIr₃ have a considerable contribution to the Fermi energy despite the stronger contribution from the Ir 5*d* states. The results of the analysis of the Ce 3*d* XAS and core-level spectra based on the single-impurity Anderson model reveal that $n_{4f} = 0.8 - 0.9$, contrast to the predictions of the previous studies [2, 9]. These results argue that the Ce 4*f* states are in an intermediate-valence state, and the contribution from the Ce 4*f* states to superconductivity is not negligible in CeIr₃.

2. Experimental Procedure

Single crystals of CeIr₃ were prepared using the Czochralski method in a tetra arc furnace under Ar atmosphere. The details of the sample growth and their characterizations were presented in Refs. [1, 3, 11]. Photoemission experiments were performed at the soft X-ray beamline BL23SU of SPring-8 [12]. The total energy resolution at the on-resonant

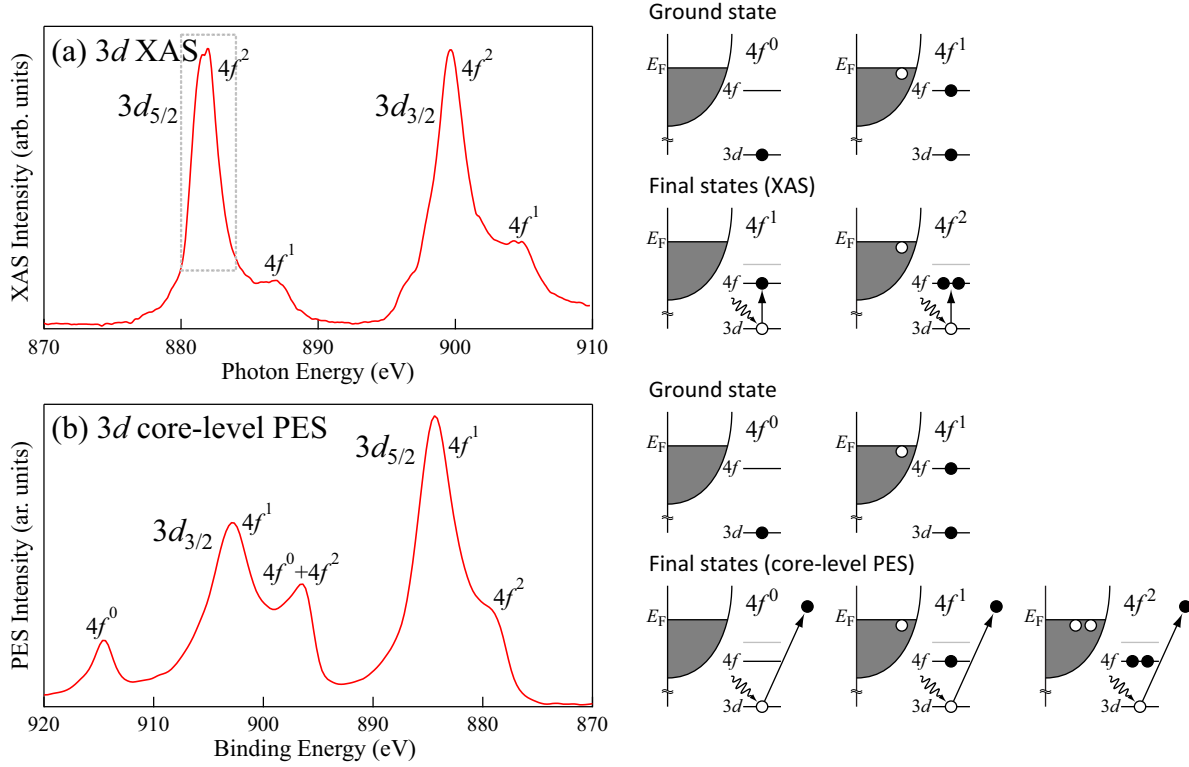


Figure 1. Ce 3d XAS and core-level spectra of CeIr₃. The schematic figures of the ground and final states in the XAS and core-level spectra are shown on the right. (a) Ce 3d XAS spectrum of CeIr₃ consisting of 3d_{5/2} and 3d_{3/2} components. Each has 4f¹ and 4f² final-state peaks. The dashed square corresponds to the region shown in Fig. 2(a). (b) Ce 3d core-level spectrum of CeIr₃ consisting of 3d_{5/2} and 3d_{3/2} components. Each has 4f⁰, 4f¹, and 4f² final-state peaks.

condition ($h\nu \sim 881$ eV) was approximately 65 meV, while that in the Ce 3d core-level measurements was approximately 190 meV. Clean sample surfaces were obtained by cleaving high-quality single crystals *in situ* under an ultra-high vacuum condition. The sample temperature was kept at 20 K during the measurements.

3. Results and Discussion

Figure 1 shows the Ce 3d XAS and core-level spectra of CeIr₃ together with the schematic figures of their ground and final states in the XAS and core-level spectra. Figure 1 (a) depicts the Ce 3d XAS spectrum of CeIr₃ consisting of 3d_{5/2} and 3d_{3/2} components. Each had 4f¹ and 4f² final-state peaks. The 4f¹ and 4f² peaks originated from the transitions from the 4f⁰ and 4f¹ configurations in the ground state, respectively. The existence of these two peaks indicated that the Ce 4f states in CeIr₃ are in an intermediate-valence state. Figure 1(b) shows the Ce 3d core-level spectrum of CeIr₃. The photon energy was $h\nu = 1200$ eV. The spectrum was essentially consistent with that in a previous XPS study [2]; however, each peak was well resolved by the better energy resolution in the present experiment. The 4f⁰ peak originates from the 4f⁰ configuration in the ground

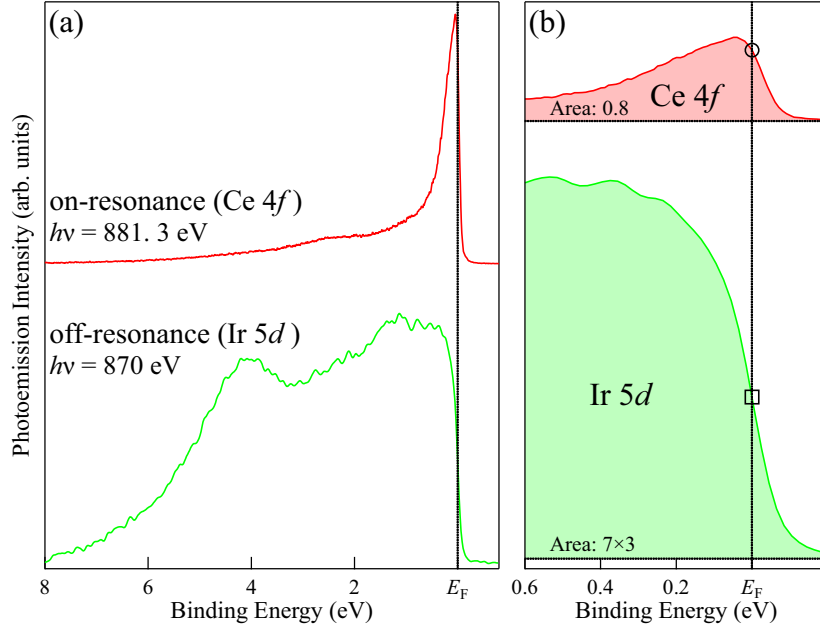


Figure 2. Resonant photoemission spectra of CeIr₃. (a) On-resonance and off-resonance photoemission spectra of CeIr₃ measured at $h\nu = 881.3$ and 870 eV, which reflect the contributions mainly from the Ce 4*f* and Ir 5*d* states, respectively. (b) On- and off-resonance spectra in the very vicinity of E_F . The areas of the spectra are normalized to the nominal numbers of electrons of the Ce 4*f* and Ir 5*d* states ($n_{4f} : n_{5d} = 0.8 : 7 \times 3$).

state. The enhanced intensity of the $4f^0$ peak again suggested that the Ce 4*f* states were in a strong mixed valence state. The calculation based on the single-impurity Anderson model suggested that $1 - n_{4f} \approx I(f^0)/[I(f^0) + I(f^1) + I(f^2)]$, where $I(f^n)$ is the $4f^n$ final-state peak intensity [13]. Thus, n_{4f} of CeIr₃ should be close to, but less than unity in the present case. The $4f^2$ final-state peak intensity was enhanced in the spectrum and was much stronger than in the case of heavy fermion compounds CeTIn₅ ($T = \text{Co, Rh, Ir}$) as an example [14]. The $4f^2$ final-state peak intensity is more enhanced in a more hybridized compound [15]; hence, the enhanced intensity in CeIr₃ indicates the existence of a strong $f - d$ hybridization in CeIr₃. The later part of this section will present a detailed analysis of these spectra.

Figure 2 summarizes the RPES measurement of CeIr₃. Figure 2 (a) shows the on- and off-resonance photoemission spectra of CeIr₃ measured at $h\nu = 881.3$ eV and $h\nu = 870$ eV, which reflects contributions mainly from the Ce 4*f* and Ir 5*d* states, respectively [16]. The Ce 4*f* states form a very sharp peak at the Fermi energy, indicating its considerable contribution to this energy. Meanwhile, a weak hump structure was found to exist around $E_B = 2.3$ eV. This was assigned to the contribution from the $4f^0$ configuration in the final state. In contrast to the Ce 4*f* states, the Ir 5*d* states form a broad band structure distributed in a wide energy range, with an overall spectral shape consistent with the GGA [2] and DFT + DMFT calculations [10]. We attempted herein to estimate the practical contributions from each orbital at the Fermi

energy. Figure 2 (b) depicts the on- and off-resonance spectra in the very vicinity of the Fermi energy. The areas of the spectra were normalized to the nominal numbers of the electrons of the Ce 4*f* and Ir 5*d* states in CeIr₃ ($n_{4f}:n_{5d} = 0.8:7 \times 3$). The Ce 4*f* and the Ir 5*d* spectra intensities can be directly compared. In practice, the occupation number of the Ce 4*f* states in CeIr₃ is estimated to be approximately 0.8 as we shall discuss later. Both the Ir 5*d* and Ce 4*f* states have considerable contributions to the Fermi energy. The contribution from the Ce 4*f* states at the Fermi energy was approximately 44 % of that from the Ir 5*d* states; thus, the contribution from the Ce 4*f* states at the Fermi energy was estimated to be approximately 31 % of the total DOS. Note that the Ce 4*f* states could form a very narrow peak at the Fermi energy, but might be smeared out by the present energy resolution (65 meV). In this case, the substantial contribution from the Ce 4*f* states may be higher than this estimation.

A further interesting point was that we found no trace of the spin-orbit-coupled 4*f*_{7/2} multiplet, located at $E_B \sim 280$ meV. The 4*f*_{7/2} multiplet originates from the final state effect, and its intensity becomes weaker than that of the peak at E_F in the Ce compound with higher Kondo temperature (T_K) [17]. Thus, the existence of the sharp peak at E_F and the absence of the 4*f*_{7/2} multiplet peak in the Ce 4*f* spectrum indicate that T_K is very high in this compound. The spectral shape of the Ce 4*f* spectrum is very similar not with the GGA calculation [2], but with the DMFT calculation [10]. This is consistent with the itinerant but correlated nature of the Ce 4*f* states in CeIr₃.

We tried qualitatively understand the Ce 3*d* core-level and XAS spectra by analyzing them based on the single-impurity Anderson model (SIAM) [18, 19, 20]. The Hamiltonian of the system is given as

$$H = H_1 + H_2 \quad (1)$$

where

$$\begin{aligned} H_1 = & \sum_{k,\nu} \varepsilon_v(k) a_v^\dagger(k, \nu) a_v(k, \nu) + \varepsilon_f^0 \sum_{\nu} a_f^\dagger(\nu) a_f(\nu) \\ & + \varepsilon_d \sum_{\mu} a_d^\dagger(\mu) a_d(\mu) + U_{ff} \sum_{\nu > \nu'} a_f^\dagger(\nu) a_f(\nu) a_f^\dagger(\nu') a_f(\nu') \\ & + \frac{V}{\sqrt{N}} \sum_{k,\nu} [a_v^\dagger(k, \nu) a_f(\nu) + a_f^\dagger(\nu) a_v(k, \nu)] \\ & - U_{fc} \sum_{\mu,\nu} a_d(\mu)^\dagger a_d(\mu) a_f^\dagger(\nu) a_f(\nu) \end{aligned} \quad (2)$$

and

$$\begin{aligned} H_2 = & \frac{1}{2} \sum_{\nu_1, \nu_2, \nu_3, \nu_4} g_{ff}(\nu_1, \nu_2, \nu_3, \nu_4) a_f^\dagger(\nu_1) a_f^\dagger(\nu_2) a_f(\nu_3) a_f(\nu_4) \\ & + \sum_{\nu_1, \nu_2, \mu_1, \mu_2} g_{fd}(\nu_1, \nu_2, \mu_1, \mu_2) a_f^\dagger(\nu_1) a_d^\dagger(\mu_1) a_d(\mu_2) a_f(\nu_2) \end{aligned}$$

$$+ \zeta_d \sum_{\mu_1, \mu_2} \alpha_{\mu_1, \mu_2} a_d^\dagger(\mu_1) a_d(\mu_2) + \zeta_f \sum_{\nu_1, \nu_2} \beta_{\nu_1, \nu_2} a_f^\dagger(\nu_1) a_f(\nu_2) \quad (3)$$

H_1 describes the SIAM with the valence band level $\varepsilon_v(k)$, 4*f* level ε_f^0 and 3*d* level ε_d . $a_v^\dagger(k, \nu)$, $a_f^\dagger(\nu)$, and $a_d^\dagger(\mu)$ are the electron creation operators in these states. k denotes the energy level index ($k = 1, 2, \dots, N$) in the valence band. ν and μ denote the combined indices to specify both the spin and orbital degeneracies of the *f* ($\nu = 1, 2, \dots, N_f$) and *d* ($\mu = 1, 2, \dots, N_d$) states with the numbers of the degeneracy of $N_f = 14$ and $N_d = 10$, respectively. H_2 represents the multiplet coupling effect described by Slater integrals F^2 , F^4 , and F^6 between 4*f* electrons (g_{ff}), the Slater integrals F^2 , F^4 , G^1 , G^3 , and G^5 between the 4*f* electrons and the 3*d* core hole (g_{fd}), and the spin-orbit interactions of the 3*d* states (ζ_d) and the 4*f* states (ζ_f). The Slater integrals were reduced down to 80% of its atomic Hartree–Fock values, which are calculated by using the Cowan program [21]. The valence band energies $\varepsilon_v(k)$ were taken as

$$\varepsilon_v(k) = \varepsilon_v^0 - \frac{W}{2} + \frac{W}{N} \left(k - \frac{1}{2}\right), \quad k = 1, 2, \dots, N, \quad (4)$$

where ε_v^0 and W are the center and width of the valence band, respectively. The N and W values were $N = 20$ and $W = 5$ eV, respectively. The 3*d* core-level ($F_{3d} \text{ XPS}(\omega)$) and 3*d* XAS ($F_{3d} \text{ XAS}(\Omega)$) spectral functions are given as follows:

$$F_{3d \text{ XPS}}(\omega) = \sum_{f, \mu} |\langle f | a_d(\mu) | g \rangle|^2 \frac{\Gamma/\pi}{(E_g + \omega - E_f)^2 + \Gamma^2} \quad (5)$$

$$F_{3d \text{ XAS}}(\Omega) = \sum_f |\langle f | T_1 | g \rangle|^2 \frac{\Gamma/\pi}{(E_g + \Omega - E_f)^2 + \Gamma^2} \quad (6)$$

where ω , Ω , and T_1 are the binding energy of the photoelectrons, photon energy, and optical dipole transition from the 3*d* to 4*f* states, respectively. Note that $|f\rangle$ in Eqs. (5) and (6) represent $N - 1$ and N electron states, respectively

Figure 3 shows the analysis result of the (a) Ce 3*d* core-level and (b) XAS spectra. We used the following parameters here: $E_F - \varepsilon_f^0 = -2.3$ eV; $U_{ff} = 7.0$ eV; $U_{fc} = 10.5$ eV; and $V = 0.5$ eV. The ratios of the 4*f*⁰, 4*f*¹, and 4*f*² configurations in the ground state were 0.111, 0.812, and 0.077, respectively. The occupation number of the Ce 4*f* states in the ground state was $n_{4f} = 0.966$. Figure 3 (a) compares the experimental Ce 3*d* core-level spectrum of CeIr₃ and the analysis result. The histogram represents the matrix elements in the calculation. The curves depict the spectra with the life-time broadening represented in Eqs. (5) and (6). The experimental spectrum was reproduced well by the SIAM using these parameters. Figure 3(b) displays the result of the Ce 3*d* XAS spectrum calculated by the same parameter set. The overall spectral shape was mostly reproduced by the calculation [18], but some discrepancies were found between the experiment and the calculation. In particular, the peak intensity of 4*f*¹ peak was weaker, and its peak position was located at the deeper-photon energy side in the calculation when compared to the experiment. To reproduce the XAS spectrum, we took a different parameter set, especially for $E_F - \varepsilon_f^0 = -2.3$ eV [22]. This problem is

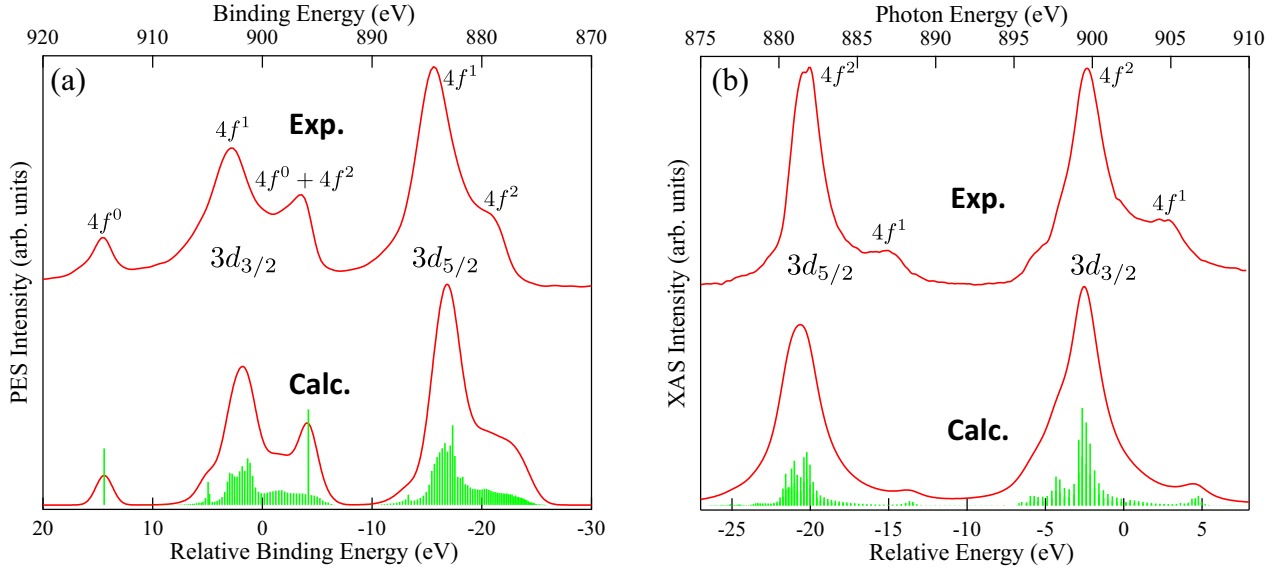


Figure 3. (a) Ce 3*d* XAS and (b) core-level spectra of CeIr₃ and their analysis results based on the SIAM. The histogram represents the matrix elements in the calculation. The curves depict the spectra with lifetime broadening represented in Eqs. (5) and (6).

presumably caused by the presence of two different Ce sites in this compound and not considered in the present analysis. Even in the case of the XAS spectrum parameters, the occupation number of the Ce 4*f* states n_{4f} was estimated to be 0.766; and thus, n_{4f} should be 0.8 – 0.9 in both cases.

Previous studies have suggested that the DOS at E_F are dominated by the Ir 5*d* states, and CeIr₃ has been considered a superconductor dominated by the Ir 5*d* bands. However, the present study revealed that the Ce 4*f* states contribute significantly to the DOS at E_F and thus to the superconductivity. Therefore, CeIr₃ is a *s*-wave superconductor with a considerable Ce 4*f* contribution as in the case of CeRu₂ [23].

Accordingly, all these results suggest that the Ce 4*f* states have an itinerant character, and a considerable contribution to the Fermi energy. The occupation number of the Ce 4*f* states n_{4f} in the ground state is estimated to be 0.8 – 0.9, which was larger than that in the previous studies.

4. Conclusion

We studied the electronic structure of CeIr₃ by the Ce 3*d* – 4*f* resonant photoelectron, Ce 3*d* XAS, and Ce 3*d* core-level spectroscopies. All experimental data suggested the well-hybridized nature of the Ce 4*f* states with the occupation number of $n_f = 0.8 – 0.9$, which was consistent with the DMFT calculation result [10]. The comparison of the intensities at the Fermi energy of the on- and off-resonance spectra suggested that more than 30 % of the DOS at the Fermi energy was contributed by the Ce 4*f* states. These results claimed a finite contribution of the Ce 4*f* states on the superconductivity of

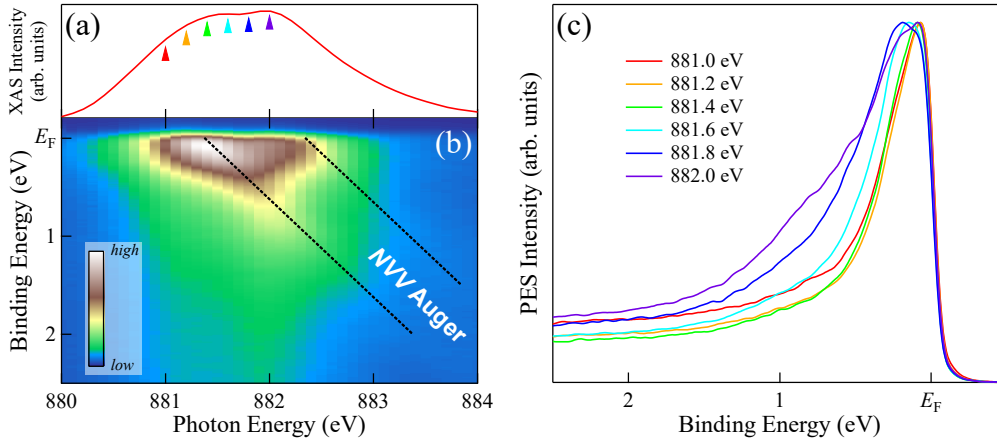


Figure A1. Resonant photoemission spectra of CeIr_3 . (a) Blowup of the Ce $4f_{5/2}$ XAS spectrum of CeIr_3 . (b) Density plot of the RPES spectra of CeIr_3 as a function of the photon energy. (c) Comparison of the RPES spectra of CeIr_3 , with intensities normalized to their maxima.

CeIr_3 . Thus, CeIr_3 is an s -wave-type superconductor with a finite contribution from the Ce $4f$ states.

Acknowledgments

The experiment was performed under Proposal Nos. 2019A3811, 2019B3811, and 2020A3811 at SPring-8 BL23SU. The present work was financially supported by JSPS KAKENHI Grant Numbers JP16H01084, JP18K03553, JP19J20539, JP20KK0061, and JP 22H03874.

Appendix A. Influence of Auger processes in RPES spectra

The contribution from the Auger signals in the resonant photoemission spectrum of the Ce-based compounds was recognized [24, 25, 26], and an appropriate selection of excitation energies is required for the measurement of the on-resonant photoemission spectrum. In this appendix, we describe the influence of Auger signals in the resonant photoemission spectra. Figures A1 (a) and (b) show the Ce $3d_{5/2}$ XAS and the density plot of the valence band spectra measured at $h\nu = 880 - 884$ eV, respectively. The gigantic resonant enhancement of the Ce $4f$ signals at the Ce $3d_{5/2}$ absorption edge was recognized at approximately $h\nu = 881 - 882$ eV. Meanwhile, two diagonal lines were recognized in Fig. A1(b), as indicated by the dotted lines, which depict the contributions from the NVV Auger signals. The resonant photoemission spectra measured at $h\nu = 881 - 882$ eV normalized by the peak height of each spectrum is displayed in Fig. A1(c) to examine the impact of the Auger signals on the Ce $4f$ spectral profiles. The spectral shapes of the resonance spectra measured at $h\nu = 881 - 881.4$ eV were almost identical, but the higher-binding-energy side of the spectrum was broadened

as the photon energy was further increased. This broadening was the contribution of the Auger signals; thus, the on-resonant spectrum should be measured at $h\nu \lesssim 881.4$ eV. We have used the incident photon energy of $h\nu = 881.3$ eV for the on-resonance spectrum to avoid the contribution from the Auger signals in the valence-band spectrum.

References

- [1] Sato Y J, Nakamura A, Shimizu Y, Maurya A, Homma Y, Li D, Honda F and Aoki D 2018 *J. Phys. Soc. Jpn.* **87** 053704
- [2] Górnicka K, Carnicom E M, Gołab S, Łapiński M, Wiendlocha B, Xie W, Kaczorowski D, Cava R J and Klimczuk T 2019 *Supercond. Sci. Technol.* **32** 025008
- [3] Sato Y J, Honda F, Shimizu Y, Nakamura A, Homma Y, Maurya A, Li D, Koizumi T and Aoki D 2020 *Phys. Rev. B* **102** 174503
- [4] Adroja D T, Bhattacharyya A, Sato Y J, Lees M R, Biswas P K, Panda K, Anand V K, Stenning G B G, Hillier A D and Aoki D 2021 *Phys. Rev. B* **103** 104514
- [5] Haldolaarachchige N, Schoop L, Khan M A, Huang W, Ji H, Hettiarachchilage K and Young D P 2017 *J. Phys. Condens. Matter* **29** 475602
- [6] Bhattacharyya A, Adroja D T, Biswas P K, Sato Y J, Lees M R, Aoki D and Hillier A D 2019 *J. Phys. Condens. Matter* **32** 065602
- [7] Górnicka K, Das D, Gutowska S, Wiendlocha B, Winiarski M J, Klimczuk T and Kaczorowski D 2019 *Phys. Rev. B* **100** 214514
- [8] Huber J 1990 *Physica B* **163** 219
- [9] Hakimi M and Huber J 1985 *Physica B+C* **135** 434
- [10] Gutowska S and Wiendlocha B 2022 *J. Magn. Magn. Mater.* **547** 168917
- [11] Sato Y J, Shimizu Y, Honda F, Nakamura A, Homma Y, Maurya A, Li D and Aoki D 2020 *JPS Conf. Proc.* **29** 011007
- [12] Saitoh Y, Fukuda Y, Takeda Y, Yamagami H, Takahashi S, Asano Y, Hara T, Shirasawa K, Takeuchi M, Tanaka T and Kitamura H 2012 *J. Synchrotron Rad.* **19** 388
- [13] Gunnarsson O and Schönhammer K 1983 *Phys. Rev. B* **28** 4315
- [14] Treske U, Khoshkhoo M S, Roth F, Knupfer M, Bauer E D, Sarrao J L, Büchner B and Koitzsch A 2014 *J. Phys. Condens. Matter* **26** 205601
- [15] Fuggle J C, Hillebrecht F U, Zolnieriek Z, Lässer R, Freiburg C, Gunnarsson O and Schönhammer K 1983 *Phys. Rev. B* **27** 7330
- [16] Yeh J and Lindau I 1985 *Atomic Data and Nuclear Data Tables* **32** 1
- [17] Kasai S, Imada S, Yamasaki A, Sekiyama A, Iga F, Kasaya M and Suga S 2007 *J. Electron Spectrosc. Relat. Phenom.* **156-158** 441
- [18] Nakazawa M, Tanaka S, Uozumi T and Kotani A 1996 *J. Phys. Soc. Jpn.* **65** 2303
- [19] Kotani A and Shin S 2001 *Rev. Mod. Phys.* **73** 203
- [20] De Groot F and Kotani A 2008 *Core level spectroscopy of solids* (CRC press)
- [21] Cowan R D 1981 *The theory of atomic structure and spectra* (Univ of California Press)
- [22] See supplementary materials for detailed information.
- [23] Kiss T, Kanetaka F, Yokoya T, Shimojima T, Kanai K, Shin S, Ōnuki Y, Togashi T, Zhang C, Chen C T and Watanabe S 2005 *Phys. Rev. Lett.* **94**(5) 057001
- [24] Cho E J, Jung R J, Choi B H, Oh S J, Iwasaki T, Sekiyama A, Imada S, Suga S, Muro T, Park J G and Kwon Y S 2003 *Phys. Rev. B* **67** 155107
- [25] Jung R J, Choi B H, Oh S J, Kim H D, Cho E J, Iwasaki T, Sekiyama A, Imada S, Suga S and Park J G 2003 *Phys. Rev. Lett.* **91** 157601
- [26] Fujimori S i 2016 *J. Phys. Condens. Matter* **28** 153002